

# Non-resonant magneto-optical effects in cold atoms

Jinyin Wan (万金银), Huadong Cheng (成华东)\*, Yanling Meng (孟艳玲),  
Ling Xiao (肖玲), Peng Liu (刘鹏), Xiumei Wang (王秀梅),  
Yaning Wang (王亚宁), and Liang Liu (刘亮)\*\*

Key Laboratory of Quantum Optics, Center of Cold Atom Physics, Shanghai Institute of Optics and Fine Mechanics,  
Chinese Academy of Sciences, Shanghai 201800, China

\*Corresponding author: chenghd@siom.ac.cn; \*\*corresponding author: liang.liu@siom.ac.cn

Received September 14, 2014; accepted November 14, 2014; posted online February 9, 2015

We report a novel nonresonant magneto-optical effect in cold atoms and present the optimized parameters of the biased magnetic field, the incident probe light intensity, and the probe detuning to obtain the maximal signal of the magneto-optical rotation. This detection scheme may further improve the stability of the cold atom clock.

OCIS codes: 020.3320, 020.1670, 290.2558.

doi: 10.3788/COL201513.020201.

The development of atomic clocks has led to many scientific and technological advances such as the Global Positioning System (GPS)<sup>[1]</sup>, the Internet (which depends critically on frequency and time standards), high-resolution spectroscopy<sup>[2]</sup>, and so on. The most accurate atomic clock uses cold atoms with a temperature close to absolute zero as the medium. Generally, the clock signals are detected by using the absorption method which produces additional background noise, thereby reducing the signal contrast and signal-to-noise ratio (SNR)<sup>[3]</sup>. In a rubidium atomic clock experimental setup<sup>[4]</sup>, Faraday rotation is used to detect the clock signal in a vapor cell to improve its contrast<sup>[5,6]</sup>. As for cold atom clocks, several methods for laser cooling of atoms have been reported. Integrating sphere cooling has a simpler structure, occupies a smaller volume, and does not require precise collimation in the cooling light<sup>[7]</sup>. These advantages render integrating sphere cooling an ideal cold atom source for a compact and small cold atom clock. We have observed the Faraday rotation signal in cold rubidium atoms in an integrating sphere which addressed the previously mentioned problem by removing the additional background noise<sup>[8]</sup>.

In this Letter, we present a different detection method with another probe light level, which brings out several desirable experimental results for rotational signals. In our previous scheme<sup>[8]</sup>, cold rubidium atoms were first obtained by a cooling laser (Toptica TA100) locked to the transition of  $5^2S_{1/2}, F=2 \rightarrow 5^2P_{3/2}, F'=3$  and a re-pumping laser (Toptica DL100) locked to the transition of  $5^2S_{1/2}, F=1 \rightarrow 5^2P_{3/2}, F'=2$ . The probe laser (Toptica TA100) transition is from  $5^2S_{1/2}, F=2$  to  $5^2P_{3/2}, F'=3$ . In this work, the probe laser transition is from  $5^2S_{1/2}, F=2$  to  $5^2P_{3/2}, F'=2$  and novel nonresonant magneto-optical effects in cold atoms in the integrating sphere are observed.

Magneto-optical effects arise when light interacts with a medium in the presence of a magnetic field  $\mathbf{B}$ <sup>[9,10]</sup>. Before and after the medium of cold atoms, two analyzers are placed with crossed optical axes acting as a blocker to

the probe light background from the photodetector (PD)<sup>[10,11]</sup>. The probe light's polarization plane is rotated as it propagates through the atomic medium placed in the longitudinal magnetic field and then the forward scattering (FS) light is detected without background noise, which is a result of the birefringence caused by the opposite displacement of the dispersion curves for the two circular polarizations ( $\sigma^\pm$ )<sup>[9,12]</sup>. If the biased magnetic field is zero, no signal can be detected. We assume ideal analyzers in this content. The FS signals for weak-intensity light can be written as<sup>[8]</sup>

$$I_{FS} = \frac{1}{4} I_0 (e^{-\alpha_+ \omega l / c} - e^{-\alpha_- \omega l / c})^2 + I_0 e^{-(\alpha_+ + \alpha_-) \omega l / c} \sin^2 \left[ \frac{(n_+ - n_-) \omega l}{2c} \right], \quad (1)$$

where  $I_0$  is the probe light intensity,  $\omega$  is the angular frequency,  $l$  is the length of the cold atom group, and  $\alpha_\pm$  and  $n_\pm$  are the absorption and refractive indices (respectively) for the  $\sigma^\pm$  components of the probe light with detuning. Since the rotation angle  $\theta$  is very small, it can be expressed as

$$\theta \approx \frac{I_{FS}}{I_0}. \quad (2)$$

Equations (1) and (2) show that the signal detected by the PD depends on the probe light detuning, the magnetic fields, and the incident probe light intensity. There is a paramagnetic effect in linear magneto-optics. The populations of the ground-state Zeeman sublevels that are split by a magnetic field are generally different in accordance with the Boltzmann distribution, which leads to a difference in the refractive indices for the corresponding light polarization components. This effect can be enhanced in the cold atom vapor through a cooling and re-pumping process by creating a nonequilibrium population

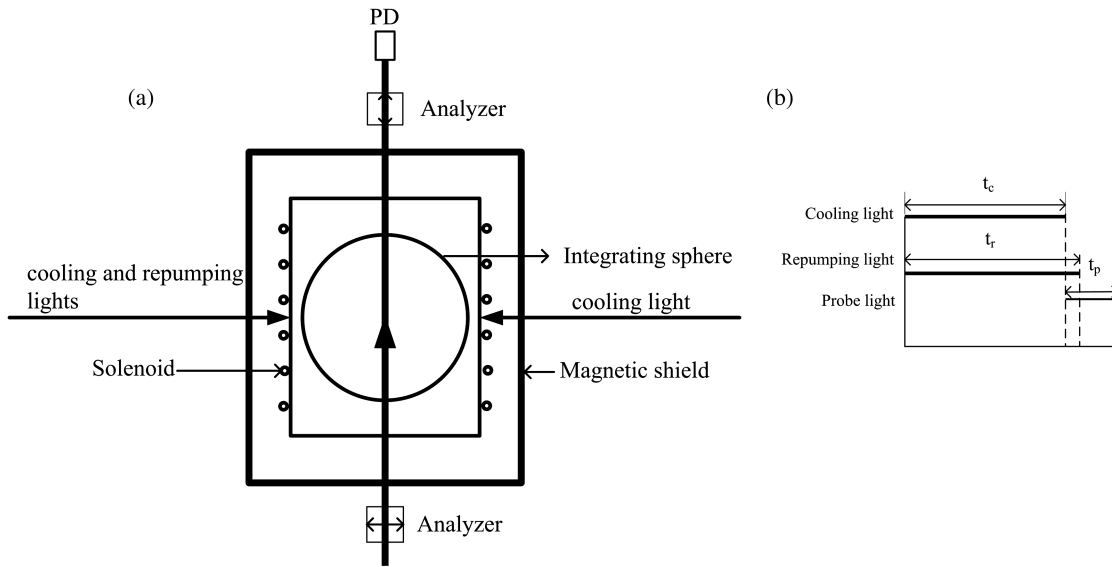


Fig. 1. (a) Experimental setup for magneto-optical detection; (b) timing sequence of the experiment. Cooling time  $t_c$  and the repumping time  $t_r$  are 177.5 and 179 ms, respectively. Probe time  $t_p$  is 7.5 ms which is switched on immediately after the cooling light is turned off.

distribution. The rotation angles' relationships with the previously mentioned parameters are studied in this work.

The experimental setup is shown in Fig. 1(a). Similarly to our previous physical system, the integrator sphere and the solenoid are placed inside the cylindrical mu-metal magnetic shield to isolate them from external magnetic fields. The solenoid wrapping around the sphere produces the longitudinal magnetic field that provides a quantization axis and lifts the Zeeman sublevel degeneracy. The two analyzers are placed before and after the physical system with crossed optical axes acting as a blocker to the probe light background from the PD. The timing sequence of this work is shown in Fig. 1(b). As for the probe light transition of  $5^2S_{1/2}, F=2$  to  $5^2P_{3/2}, F'=2$ , it is not a closed transition, because the excited state  $5^2P_{3/2}, F'=2$  would spontaneously decay to the levels  $5^2S_{1/2}, F=2$  and  $F=1$ , so the repumping light should remain on for a period of time after the cooling light is off (as well as in the initial time period of the probe light being switched on) to keep the atoms in the state of  $5^2S_{1/2}, F=2$  or there will be no signal. In the experiment, the cooling time  $t_c$  and the repumping time  $t_r$  are 177.5 and 179 ms, respectively. The probe time  $t_p$  is 7.5 ms which is switched on immediately after the cooling light being off.

The power of the two cooling lights which travel along the opposite directions is 130 mW, and the power of the repumping light is 5.5 mW. We can explore the rotation angle versus the magnetic field according to Eqs. (1) and (2). The probe light's detuning is set as a red detuning  $-3.9$  MHz and its diameter is 4 mm for detection. The magnetic field is from 0 to 34.2 mG. Since the rotation angle depends on the transmitted probe light intensity (which is obtained through the probe light power divided by the cross sectional area), the time-dependent signals (Fig. 2) show that the magnetic field is 20.6 and 0 mG

(solid and dashed lines, respectively). The transmitted signal is calculated through the maximum minus the minimum value. It shows that there is repumping light leakage under the zero magnetic field condition in which the pure transmitted intensity should be zero. Then each pure transmitted signal is obtained by subtracting the corresponding zero magnetic field transmitted signal.

The transmitted rotation angles of the linear probe light versus the magnetic fields at different intensities of the probe light are shown in Fig. 3 (where the uncertainty of the data points is 5%). It is clearly seen that when the magnetic field is zero there is no transmitted signal, and the rotation angles decrease as the incident probe

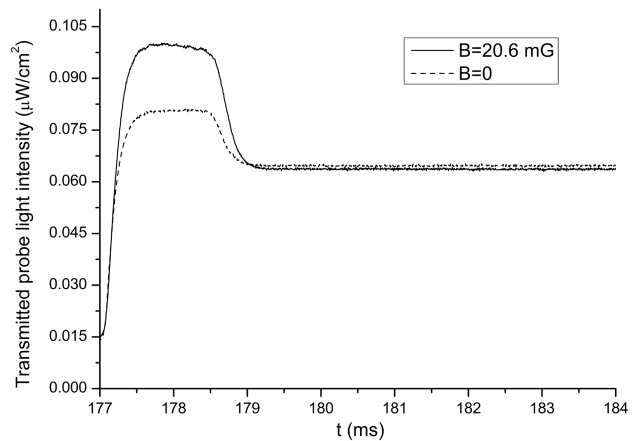


Fig. 2. Transmitted probe light intensity when the biased magnetic field is 20.6 and 0 mG (solid and dashed lines, respectively). There is repumping light leakage at  $\mathbf{B}=0$ ; pure transmitted probe light intensity is obtained by subtracting such repumping light leakage.

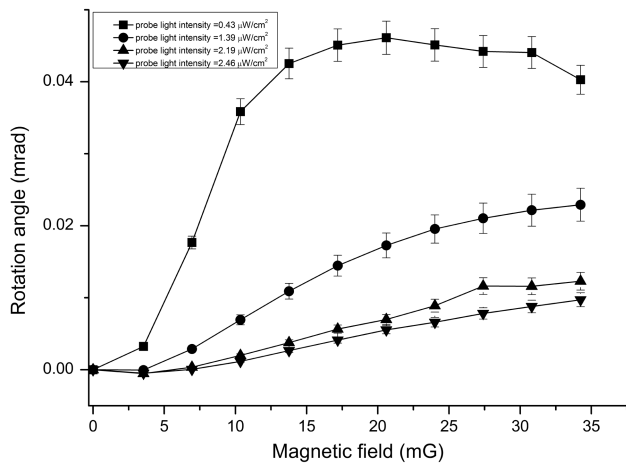


Fig. 3. Rotation angle versus the biased magnetic fields at different incident probe powers where the uncertainty of the data points is 5%. Probe light transition is from  $5^2S_{1/2}, F=2$  to  $5^2P_{3/2}, F'=2$ . Magnetic field is from 0 to 34.2 mG. Incident probe intensities are 0.43, 1.39, 2.19, and 2.46 mW/cm<sup>2</sup>. Largest rotation angle is 0.046 mrad when the magnetic field is 20.6 mG and the probe light intensity is 0.43 mW/cm<sup>2</sup>.

light intensities increase. Furthermore, when the probe light intensity is 0.43 mW/cm<sup>2</sup>, the profile is nonlinear and the largest rotation angle of 0.046 mrad is at about 20.6 mG. When the probe light intensity is greater than 1.39 mW/cm<sup>2</sup>, the profile is nearly linear. Equations (1) and (2) show that  $\theta$  is linear in accordance with  $\mathbf{B}$  at small values of the field, peaks at a value, and falls off in the limit of large fields. Figure 3 demonstrates such a phenomenon; with the increase of the incident probe light intensity, a larger field is needed to reach the peak. As for larger probe light intensities of 2.19 and 2.46 mW/cm<sup>2</sup>, the trend is nearly linear from 3.5 to 27.5 mG. For a small probe light intensity, hardly any linear region is seen but the rotation angle is larger than that of the high intensities, so the parameters such as the magnetic field and the probe light intensity need to be optimized to obtain higher rotation angles that correspond to the magneto-optical effect.

The magnetic field was set as 20.6 mG to investigate the rotation angle versus the probe light intensity (Fig. 4), where the uncertainty of the data points is 5%. Figure 4 shows the rotation angle versus the probe light power at detunings of 0,  $-3.9$ , and  $-6.3$  MHz. It can be seen that the profiles are similar for different probe detunings. The maximum is at about 0.31 mW/cm<sup>2</sup> and then decreases slowly.

We then set the magnetic field at 20.6 mG and the incident power at 0.31 mW/cm<sup>2</sup>. Figure 5 demonstrates the rotation angle versus the probe laser detuning where the uncertainty of the data points is 5%; the profile presents a broad asymmetric peak shape and the maximum value of 0.087 mrad is at a red detuning  $-3.9$  MHz.

In conclusion, we present nonresonant magneto-optical effects in cold rubidium atoms in an integrating sphere. The rotation angle of the linear polarized probe light at different magnetic fields, the incident probe

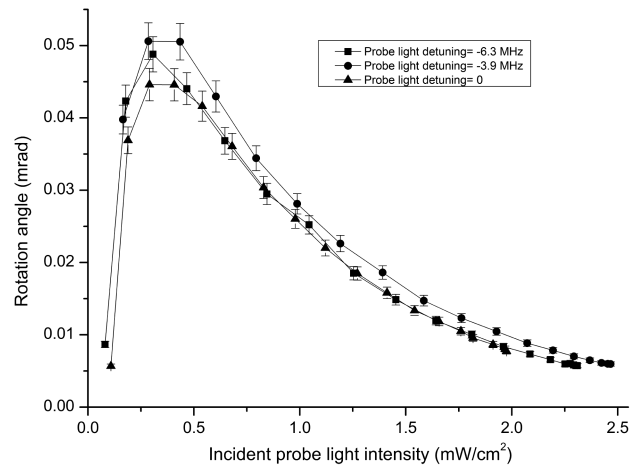


Fig. 4. Rotation angle versus the probe light intensity where the uncertainty of the data points is 5% at different detunings 0,  $-3.9$ , and,  $-6.3$  MHz, respectively. Probe light transition is from  $5^2S_{1/2}, F=2$  to  $5^2P_{3/2}, F'=2$ , and the magnetic field is set as 20.6 mG. Profiles are similar as for different probe detunings; there is a peak at about 0.31 mW/cm<sup>2</sup> and then decreases slowly.

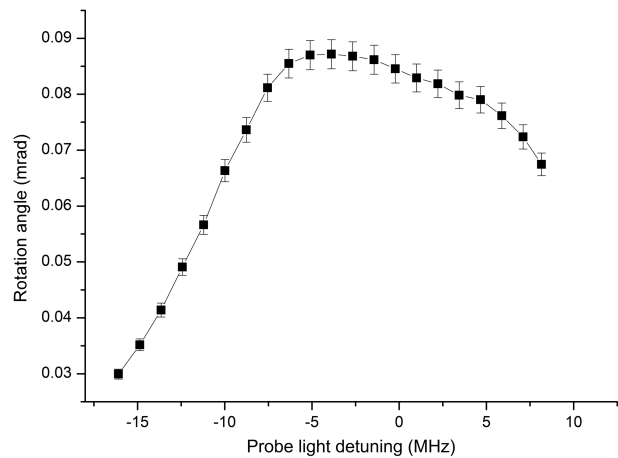


Fig. 5. Rotation angle versus probe light detuning where the uncertainty of the data points is 5%. Probe light transition is from  $5^2S_{1/2}, F=2$  to  $5^2P_{3/2}, F'=2$ . Magnetic field is 20.6 mG and the incident power is 0.31 mW/cm<sup>2</sup>. Maximum rotation angle of 0.087 mrad is at red detuning  $-3.9$  MHz.

power, and the probe detuning are demonstrated. It is found that the rotation angle profiles versus incident probe power are similar for different probe detunings, and the value is nearly fixed from a red detuning 5 MHz to the resonant frequency. The probe scheme of  $5^2S_{1/2}, F=2$  to  $5^2P_{3/2}, F'=2$  is insensitive to the power and frequency of the probe light for cold atom clock signal detection. This detection scheme may further improve the stability of the cold atom clock.

This work was supported by the National Natural Science Foundation of China (No. 11034008) and the National High-Tech Research and Development Program of China (No. 2012AA120702).

**References**

1. S. Knappe, V. Shah, P. D. D. Schwindt, L. Hollberg, J. Kitching, L. A. Liew, and J. Moreland, *Appl. Phys. Lett.* **85**, 1460 (2004).
2. C. Chin, V. Vuletić, A. J. Kerman, and S. Chu, *Phys. Rev. Lett.* **85**, 2717 (2000).
3. S. A. Zibrov, I. Novikova, D. F. Phillips, R. L. Walsworth, A. S. Zibrov, V. L. Velichansky, A. V. Taichenachev, and V. I. Yudin, *Phys. Rev. A* **81**, 013833 (2010).
4. Y. Ma, J. Deng, Z. Hu, H. He, and Y. Wang, *Chin. Opt. Lett.* **11**, 032701 (2013).
5. J. D. Lin, J. L. Deng, Y. S. Ma, H. J. He, and Y. Z. Wang, *Opt. Lett.* **37**, 5036 (2012).
6. J. D. Lin, J. L. Deng, H. J. He, and Y. Z. Wang, *Appl. Opt.* **52**, 2169 (2013).
7. H. D. Cheng, W. Z. Zhang, H. Y. Ma, L. Liu, and Y. Z. Wang, *Phys. Rev. A* **79**, 023407 (2009).
8. B. C. Zheng, H. D. Cheng, Y. L. Meng, L. Xiao, J. Y. Wan, and L. Liu, *Chin. Phys. Lett.* **31**, 073701 (2014).
9. D. Budker, W. Gawlik, D. F. Kimball, S. M. Rochester, V. V. Yashchuk, and A. Weis, *Rev. Mod. Phys.* **74**, 1153 (2002).
10. A. Corney, B. P. Kibble, and G. W. Series, *Proc. R. Soc. London A* **293**, 70 (1966).
11. W. Gawlik, J. Kowalski, R. Neumann, and F. Träger, *Opt. Commun.* **12**, 400 (1974).
12. C. Wieman and T. W. Hänsch, *Phys. Rev. Lett.* **36**, 1170 (1976).